Impact of Sensor Data Sampling Rate in GNSS/INS Integrated Navigation with Various Sensor Grades

Yida. Wei [1], You. Li [2,3] *

[1] School of Geodesy and Geomatics, Wuhan University, Wuhan, China - yiida@qq.com
[2] State Key Laboratory of Information Engineering in Surveying, Mapping and Remote Sensing, Wuhan University, Wuhan, China - liyou@whu.edu.cn
[3] Hubei Luojia Laboratory, Wuhan, China

Commission III, WG III/1

KEY WORDS: Sampling Rate, Positioning Accuracy, Power-Accuracy Trade-off, GNSS/INS, Low Power Consumption

ABSTRACT:

The fast-growing small-size equipment requires robust navigation with low power consumption and high positioning accuracy. However, as the mainstream robust navigation method against different environments, GNSS/INS causes excessive power dissipation. Considering downsampling is confirmed as a simple but efficient way to reduce energy usage, this paper focuses on the impact of sensor data sampling rate in GNSS/INS integrated navigation to give guidance for selecting proper GNSS/INS rates. Specifically, we first simulated data sequences with various sensor grades and then downsampled them into multiple sampling rates, followed by positioning accuracy evaluation. Experiment results have shown that GNSS interval caused more significant degradation of the navigation accuracy than the IMU rate. Meanwhile, the 5 sec GNSS interval with the 20 Hz IMU rate may be the most suitable for a power-accuracy trade-off solution in our experiments, which has a 16% reduction in positioning accuracy compared to the standard sampling rate combination (i.e, 1 sec GNSS interval and 200 Hz IMU sampling rate).

1. INTRODUCTION

With the rapid development of small-size equipment and the surging needs of intelligent cities, robust, high-accuracy, low-power navigation in mobile and embedded devices are in great demand in various scenarios, such as wearable positioning systems. The major approach to achieve high accuracy and robustness against different environments is adopting a global navigation satellite system (GNSS)/inertial navigation system (INS) integrated navigation system, which complementarily combines GNSS for external-reference long-term positioning and INS for internal-derivation short-term positioning. However, GNSS/INS, while boosting positioning accuracy and robustness, will unavoidably have high computational loads and more energy consumption, leading to possible unsuitability for devices with rigid power restrictions, like smartphones and internet-of-things (IoT) devices. Besides, different manners and degrees of power reduction have various influences on positioning accuracy. Therefore, to achieve robust navigation and meet both power and accuracy needs for small-size equipment, it is essential but challenging to find a power-accuracy trade-off point in GNSS/INS integrated navigation.

Various methods to reduce the power consumption of integrated navigation systems are proposed by reducing the computation load, which are generally divided into improving the inertial navigation algorithm and simplifying the Kalman filtering (Yan, 2021). Zhang et al. reduced the computation efforts by omitting computation terms of the INS navigation equation like rotation correction and sculling correction that have little influence on the accuracy confirmed by quantitative analysis (Zhang, 2013). Yan et al. proposed an integrated navigation algorithm with multi-power adaptive capability through simplified equations, which can reduce the clock frequency of the microcontroller unit (Yan, 2021). The above methods have also proposed low-power solutions considering down-sampling the inertial measurement unit (IMU) to a low rate, such as 10 Hz. Considering decreasing sampling frequency is regarded as a simple but efficient way to reduce power consumption (Dieter, 2005), research on choosing a reasonable lower rate is necessary.

To select a suitable sampling rate for scenes with different accuracy and power consumption requirements, a few works conducted a quantitative study about the impact of sensor data sampling frequency on positioning accuracy. Zhang et al. assessed the effect of high (50 Hz) and low (1 Hz) GNSS sampling rates on GNSS/INS through Allan variance and guided the reasonable selection of GNSS sampling rates to meet the demands (Zhang, 2019). Lee and Choi analyzed the effect of the strap-down integration order and sampling rate on the attitude estimation accuracy for low-cost IMU applications (Lee, Choi, 2018). Among them, reducing sampling frequency will sacrifice accuracy. However, these works mainly focus on the relationship between the single sampling rate of INS or GNSS and the single performance of accuracy or power. It remains a unified and quantitative investigation for a more appropriate selection of GNSS and IMU sampling rates to meet the demands of high-accuracy GNSS/INS in low-energy equipment.

To tackle the issues above, this paper mainly concentrates on the impact of the sampling frequency combinations of GNSS

* Corresponding author

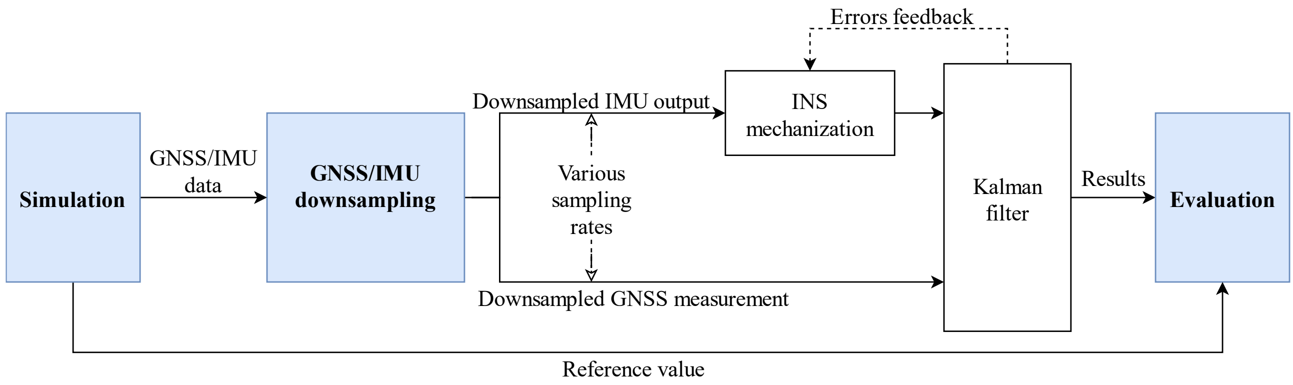

Figure 1. Flowchart of experiment scheme. Our work is in blue.

and IMU on power consumption and positioning accuracy by experiments concerning various scenarios. However, different sensor grades, movement trajectories, and vehicles may have different selections of an accuracy-power trade-off sampling rate while it is of high workloads to implement experiments for all scenarios in the real world. Therefore, the experimentations will be based on a GNSS/INS simulation software (AINS-SIMU) developed by the GNSS Research Center at Wuhan University to conveniently and efficiently set specific scenes at zero cost.

The scheme of our experiment is illustrated in Figure 1. First, AINS-SIMU simulates multi-precision data for both GNSS and IMU. In particular, these data contain real-time kinematic (RTK) (5 cm position accuracy) and standard point positioning (SPP) position data (1 m position accuracy) for GNSS, and tactical-grade (1 deg/h gyro bias) and consumer-grade (300 deg/h gyro bias) INS data. Then, the GNSS/INS data is downsampled with multiple sampling rates, followed by putting the downsampled GNSS data and INS data (after INS mechanization) into Kalman filter for trajectory calculation in AINS (Aided Inertial Navigation System, an integrated navigation program). Finally, we evaluate positioning accuracy and comprehensively analyze the relationship between precision, sampling rate, power, and accuracy.

2. NAVIGATION ALGORITHM

The most popular GNSS/INS integration scheme is loosely coupled, where the position and velocity derived from GNSS signal processing are merged into an update of the INS estimated position information through a Kalman filter (Aggarwal and Priyanka, 2010). In our work, the downsampled data will be processed by a loosely-coupled GNSS/INS integration algorithm.

2.1 System State Estimation

The Kalman filter state vector contains navigation state errors and sensor errors given in (1).

$$\delta\boldsymbol{x}(t) = \left[(\delta\boldsymbol{r}^n)^T \quad (\delta\boldsymbol{v}^n)^T \quad \boldsymbol{\phi}^T \quad \boldsymbol{b}_g^T \quad \boldsymbol{b}_a^T \quad \boldsymbol{s}_g^T \quad \boldsymbol{s}_a^T\right]^T, \tag{1}$$

where $\delta\boldsymbol{r}^n$ = inertial navigation position error vector
$\delta\boldsymbol{v}^n$ = inertial navigation velocity error vector
$\boldsymbol{\phi}$ = inertial navigation attitude error vector
$\boldsymbol{b}_g$ = tri-axis gyroscope bias
$\boldsymbol{b}_a$ = tri-axis accelerometer bias
$\boldsymbol{s}_g$ = tri-axis gyroscope scale factor error
$\boldsymbol{s}_a$ = tri-axis accelerometer scale factor error

According to the continuous-time differential equation, after deriving the derivative for $\delta\boldsymbol{x}(t)$, the obtained error model is illustrated by the sequence of differential equations as stated in (2) (El-Sheimy, 2004).

$$\begin{aligned} \delta\dot{\boldsymbol{r}}^e &= \delta\boldsymbol{v}^e\ ; \\ \delta\dot{\boldsymbol{v}}^e &= \boldsymbol{N}\delta\boldsymbol{r}^e - 2\boldsymbol{\Omega}_{ie}^e\delta\boldsymbol{v}^e - \boldsymbol{F}^e\boldsymbol{\phi}^e + \boldsymbol{C}_b^e\delta\boldsymbol{f}^b\ ; \\ \dot{\boldsymbol{\phi}} &= -\boldsymbol{\Omega}_{ie}^e\boldsymbol{\phi}^e + \boldsymbol{C}_b^e\delta\boldsymbol{\omega}_{ib}^b\ , \end{aligned} \tag{2}$$

where “dots” denote the time derivatives; the superscript “e” and “b” denote the e-frame (i.e., the Earth-Centered, Earth-Fixed frame), and the b-frame (i.e., the body frame) (Godha, 2006),
$\boldsymbol{N}$ = tensor of the gravitational gradients
$\boldsymbol{\Omega}_{ie}$ = skew-symmetric matrix of the Earth rotation rate relative to inertial space
$\boldsymbol{F}$ = skew-symmetric matrix of specific force
$\boldsymbol{C}_b^e$ = rotation matrix from b-frame to e-frame
$\delta\boldsymbol{f}$ = output errors of accelerometer
$\delta\boldsymbol{\omega}_{ib}$= output errors of gyroscope

Gyro and accelerometer biases and scale factor errors are modeled as first-order Gauss-Markov processes as

$$\begin{cases} \dot{\boldsymbol{b}}_g(t) = -\frac{1}{T_{gb}}\boldsymbol{b}_g(t) + \boldsymbol{w}_{gb}(t) \\ \dot{\boldsymbol{b}}_a(t) = -\frac{1}{T_{ab}}\boldsymbol{b}_a(t) + \boldsymbol{w}_{ab}(t) \\ \dot{\boldsymbol{s}}_g(t) = -\frac{1}{T_{gs}}\boldsymbol{s}_g(t) + \boldsymbol{w}_{gs}(t) \\ \dot{\boldsymbol{s}}_a(t) = -\frac{1}{T_{as}}\boldsymbol{s}_a(t) + \boldsymbol{w}_{as}(t) \end{cases}, \tag{3}$$

where T = correlation time of first-order Gauss-Markov processes
w = white noise of first-order Gauss-Markov processes

2.2 GNSS Observation Equation

The GNSS position observation equation is used as the measurement update of the Kalman filter, and the measurement equation is given in (4) (Li, 2015).

$$\mathbf{z} = \hat{\mathbf{r}}_{\mathrm{INS}}^{\mathrm{e}} - \tilde{\mathbf{r}}_{\mathrm{GNSS}}^{\mathrm{e}} = \boldsymbol{\delta}\mathbf{r}^{\mathrm{e}} + \mathbf{V}_{\mathrm{r}}\ , \tag{4}$$

where $\hat{\mathbf{r}}_{\mathrm{INS}}^{\mathrm{e}}$ = the position vector predicted by INS mechanization
$\hat{\boldsymbol{r}}_{INS}^{e}$ = the position vector provided by GNSS
$\mathbf{V}_r$ = measurement noise

https://doi.org/10.5194/isprs-archives-XLVI-3-W1-2022-205-2022 | © Author(s) 2022. CC BY 4.0 License.

3. ANALYSIS METHOD

The simulation analysis consists of three steps: simulation, downsampling, and accuracy evaluation. First, we simulate multi-precision data for both GNSS and IMU. Then the GNSS/INS data is downsampled with multiple sampling rates for navigation. Finally, we evaluate positioning accuracy statistically.

3.1 Simulation

As mentioned in Section 1, the simulation process is completed by AINS-SIMU. The work module of the simulator is shown in Figure 2 (Li, 2012). GNSS/INS performance and trajectory information settings are put into the simulator, then the simulator exports the reference navigation information (i.e., position, velocity, and attitude), GNSS measurements, and IMU outputs.

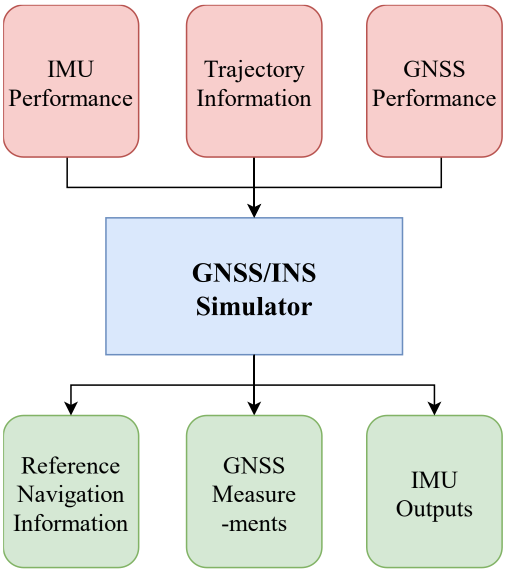

Figure 2. Block diagram of the simulator.

3.2 Downsampling

After acquiring the simulation navigation data, we downsample the data into various sampling rates to imitate a simplified non-real-time processing case, then input the pre-processed data to the positioning software.

It was evident that when reducing the sampling rate of GNSS, the navigation results will drift with time more significantly. With a lower rate of the GNSS correction, the period of single INS estimation gets extended, thus accumulating larger velocity and attitude errors and then degrading the positioning accuracy (Niu, 2010).

During the INS-mechanization process, to model the motions of vehicles, some changes are regarded as happening in a short time Δt (i.e., Δt approaches zero), such as the location changes and the attitude changes (Noureldin, 2013). While reducing the INS sampling rates, Δt will become longer, bringing more significant uncertainty, so the assumption that the change is a minor amount may lead to a larger error.

3.3 Evaluation

Following the above, the position errors that measure the accuracy of navigation results can be skillfully defined as the deviation between the reference position from the simulator and the estimated position from the Kalman filter. We give a statistical summary of position errors through the root mean square (RMS). For the rate of Kalman filter output is in common with the INS sampling rate, different INS frequencies may have different rates of navigation results. Thus, we calculate the RMS of every data group in common points.

4. SIMULATION TESTS AND RESULTS

4.1 Simulation Tests

Two different grades of IMU were simulated in this paper. The first was FSAS tactical-grade IMU with 1 deg/h gyro bias, and the other was MTi-G consumer-grade IMU with 300 deg/h gyro bias. Meanwhile, two different performances of GNSS including RTK with 5 cm position accuracy and SPP with 1 m position accuracy were simulated. The specific descriptions of the simulated sensor accuracy are given in Table 1 and Table 2, respectively.

	Simulated errors	**FSAS** (tactical-grade)	**MTi-G** (consumer-grade)
IMU	Gyro bias instability	σ=0.75 deg/hr，τ=4 hr	σ=360 deg/hr，τ=100 sec
	Gyro white noise (ARW)	0.1 deg/sqrt(hr)	3 deg/sqrt(hr)
	Gyro scale factor instability	σ=300 PPM	σ=3000 PPM
	Accel. bias instability	σ=1000 mGal, τ=4 hr	σ=3000 mGal，τ=100 sec
	Accel. white noise (VRW)	0.03 m/s/sqrt(hr)	0.12 m/s/sqrt(hr)
	Accel. Scale factor instability	σ=300 PPM	σ=3000 PPM
	Data rate	200 Hz	200Hz

Table 1. IMU performance configuration. Sensor biases are modeled as first-order Gauss-Markov processes.

	Simulated errors	**RTK**	**SPP**
GNSS	Position instability	σ=0.05 m	σ=3 m
	Data rate	1 Hz	1Hz

Table 2. GNSS performance configuration.

Four types of the GNSS and INS combination are as follows:

1. RTK + FSAS;
2. SPP + FSAS;
3. RTK + MTi-G;
4. SPP + MTi-G.

The trajectories of the above modes described in Table 3 were designed to cover a variety of vehicle motion types, such as uniform linear motion, uniformly accelerated linear motion, variable acceleration motion, uniform circular motion, and variable angular velocity motion so that we can analyze the impact of sampling rates in diverse situations (Li, 2015). The track is visualized in Figure 3.

Also, a set of real-world collected data is used in this experiment, including the stationary state and linear motion state. The sensor accuracy and the estimating trajectory of real data are given in Table 4 and Figure 4, respectively.

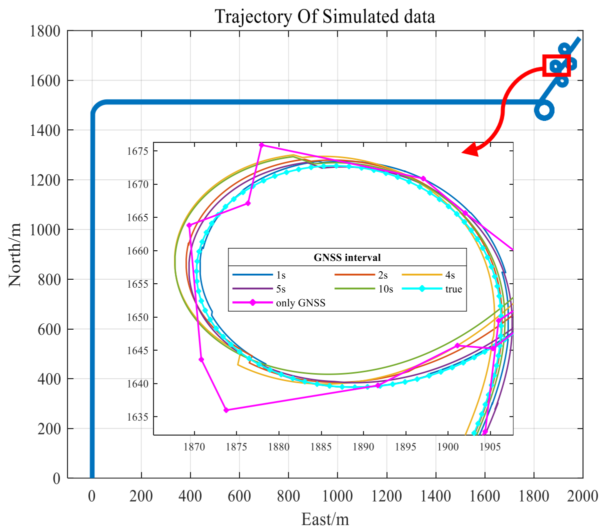

Figure 3. Simulated trajectory (configuration: SPP + FSAS).

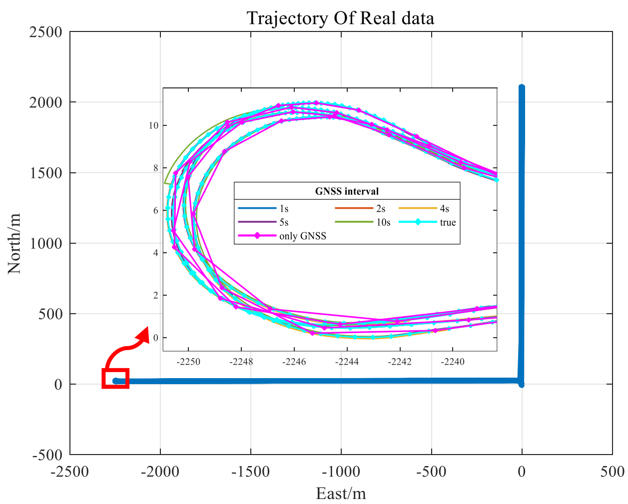

Figure 4. Real collected trajectory.

Time segment (Sec)	**Motion description**
0-100	Static
100-110	Forward velocity increases linearly in time (acceleration = 2 m/s^2)
110-170	Uniform linear motion (speed = 20 m/s)
170-180	Forward velocity decreases linearly in time (acceleration = -1 m/s^2)
180-190	Turn 90 degrees with constant angular acceleration
190-220	Uniform linear motion (speed = 10 m/s)
220-280	Motion with sinusoidal varying forward acceleration (forward acceleration changes with Amplitude = 4 m/s^2 and Period = 20 s)
280-290	Uniform linear motion (speed = 10 m/s)
290-350	The first three-second angular velocity rises from 0 to 18 deg/s; then uniform angular motion (angular velocity =18 deg/s); the last three-second angular velocity falls to 0
350-360	Uniform linear motion (speed = 10 m/s)
360-420	Motion with sinusoidal varying angular velocities (speed = 10 m/s; angular velocity changes with Amplitude = 36 deg/s and Period = 20 s)
420-430	Forward velocity decreases linearly in time (acceleration = -1 m/s^2)
430-530	Static

Table 3. Description of the trajectory.

	Errors	**Values**
GNSS	Position instability	RTK: σ=0.05 m SPP: σ=3 m
	Data rate	1 Hz
IMU	Gyro bias	0.0035 deg/hr
	Gyro bias variation	0.00175 deg/hr
	Gyro white noise (ARW)	0.0025 deg/sqrt(hr)
	Gyro scale factor error	5 PPM
	Accel. bias	30 μg
	Accel. bias variation	15 μg
	Accel. white noise (VRW)	1.3 μg/sqrt(Hz)
	Accel. Scale factor error	100 PPM
	Axes misalignment	5 arcsec
	Data rate	200 Hz

Table 4. Real-world sensor accuracy.

Mode / GNSS interval	REAL RMS (m)	RTK+FSAS RMS (m)	SPP+FSAS RMS (m)	RTK+MTi-G RMS (m)	SPP+MTi-G RMS (m)
1 s (standard)	0.446	0.091	1.838	0.142	4.204
2 s	0.447	0.142	2.572	0.265	5.853
4 s	0.460	0.480	3.468	0.479	7.932
5 s	**0.502**	**0.682**	**3.199**	**0.896**	**9.415**
10 s	0.967	0.950	4.385	4.771	17.311
30 s	11.949	0.942	5.632	119.123	126.672

Table 5. Positioning errors under various GNSS intervals; unit: m.

4.2 Results and Analysis

From experience, the location applications based on GNSS become the top power-hungry apps due to the high processing and communication costs (Lo'ai A. Tawalbeh, 2016). Therefore, we firstly choose a proper GNSS sampling rate that minimizes power consumption while meeting accuracy.

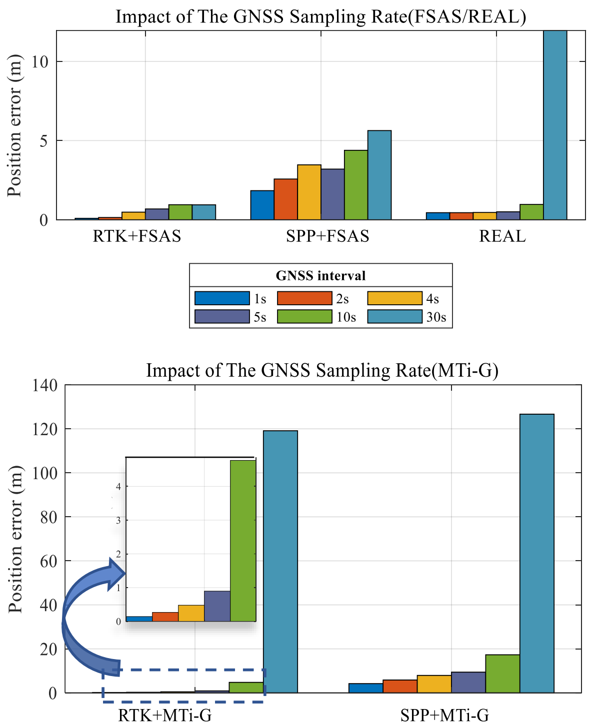

Figure 5. Impact of GNSS sampling rate on positioning accuracy.

Figure 5 shows the impact of the GNSS sampling rate on positioning accuracy. Also, the three-dimensional RMS of the navigation results is given in Table 5. It can be seen that long GNSS gaps reduce the positioning accuracy distinctly. Moreover, the GNSS sampling rate has a more noticeable impact on MTi-G, the consumer-grade IMU, which dramatically degrades especially when the GNSS interval is 30 sec. In this experiment, 5 sec GNSS interval with lower consumption than the shorter interval can maintain about 10 m accuracy even at the lowest sensor level (SPP + MTi-G). Therefore, we choose the GNSS rate of 0.2 Hz to be an appropriate choice in the follow-up tests.

It should be noted that the simulated data rate is 200 Hz, which is lower than the real-world data rate in a high frequency. While reducing the IMU sampling rate, the simulated data may not reflect the correct results very well. Therefore, we will focus on the real-world collected data to analyze the impact of the IMU sampling rate.

Figure 6 shows the partial trajectory of the navigation results with various IMU sampling rates. For real-world data, we regarded the smoothing navigation results as the reference value.

As shown in Figure 6, when the vehicle turned around, the extent to which the predicted position deviated from the reference value increased as the sampling rate decreased. Moreover, when the vehicle began to move in an approximately linear motion, the impact of the various IMU sampling rates became more inconspicuous. According to the inference in Section 3, IMU downsampling may increase the position error because of the approximate processing, and turning around usually means greater acceleration and angular velocity, which magnifies the error caused by the proximate processing.

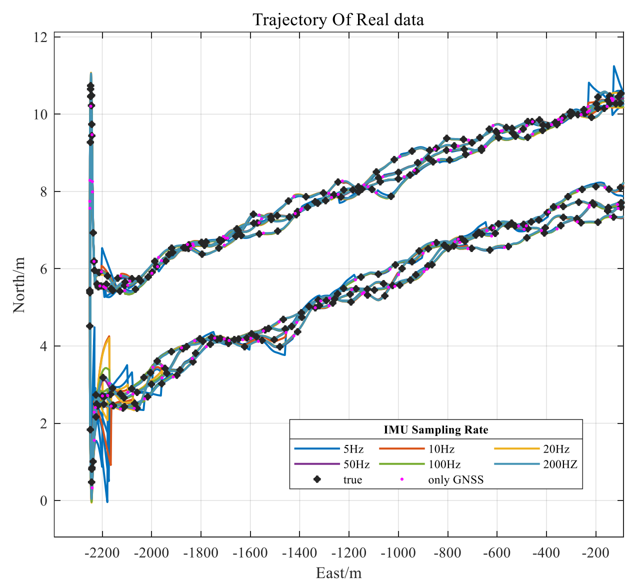

Figure 6. Partial trajectory of navigation results; GNSS interval: 5 sec.

Figure 7 shows the impact of the IMU sampling rate while the GNSS interval is 5 sec.

https://doi.org/10.5194/isprs-archives-XLVI-3-W1-2022-205-2022 | © Author(s) 2022. CC BY 4.0 License.

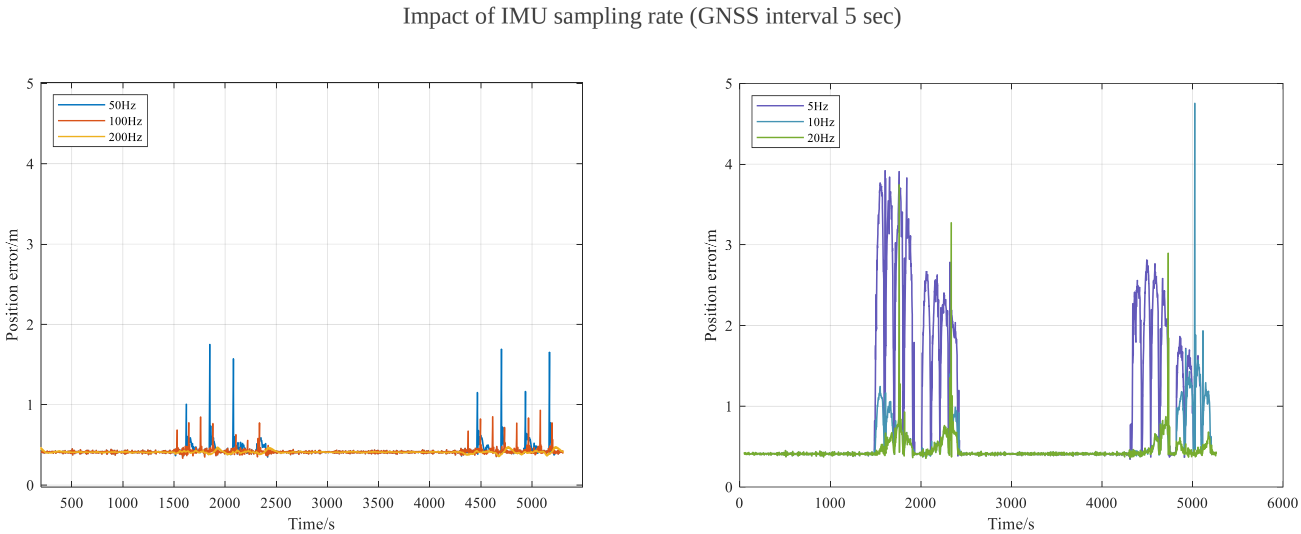

Figure 7. Impact of the IMU Sampling Rate on positioning accuracy; GNSS interval 5 sec.

Mode / IMU Sampling rate	**REAL** RMS (m)
200 Hz (standard)	0.502
100 Hz	0.483
50 Hz	0.507
20 Hz	**0.520**
10 Hz	0.600
5 Hz	1.273

Table 6. Positioning errors under various IMU sampling rates; GNSS interval: 5 sec; unit: m.

As illustrated in Figure 7, the experiments based on the real-world data showed the same trend as expected. From 200 Hz IMU rate to 10 Hz IMU rate, the uptrend of position error is slow, while the 5 Hz IMU rate causes a significant degradation. Meanwhile, it is obvious that during the static period, the IMU sampling rate has little influence on the positioning accuracy, which is in line with the anticipation. The precise comparison by the statistic summary of the position errors is shown in Table 6.

It can be seen from Table 6 that the 100 Hz IMU had little influence on the positioning accuracy while the 5Hz IMU rate reduced that by about 153%. Consequently, 200 Hz or 100 Hz may be good choices for a high accuracy demand, while 5 Hz decreasing 97.5% computation load meets the low power consumption need. Meanwhile, the 20Hz IMU sampling rate that reduced the accuracy by approximately 3% and decreased 90% power consumption can be a power-accuracy trade-off solution for our experiments. Compared with Table 5, the combination of the 5 sec GNSS interval and the 20 Hz IMU sampling rate reduced the positioning accuracy by about 16%.

5. CONCLUSION

In this paper, the impact of sensor data sampling rate in GNSS/INS was analyzed by experiments with simulated data and real-world data. In our experiments, the GNSS sampling rate significantly affected the positioning accuracy. Because of the dramatic uptrend of position errors from 5 sec GNSS interval to 10s GNSS interval, we choose the GNSS interval as 5 sec (i.e., 0.2 Hz GNSS sampling rate). Through a precise comparison, we found that the 20 Hz IMU sampling rate with 90% power consumption decreasing and 3% positioning accuracy degradation is more appropriate for our experiments. The final result shows that 5 sec GNSS interval and 20 Hz IMU sampling rate combination decreased the positioning accuracy by 16%. This paper has shown that sometimes downsampling with the acceptable accuracy degradation is a feasible way to reduce the power consumption and provide initial guidance for choosing sampling rates that meet navigation needs.

Future works will focus on acquiring broader results through the investigation of more types of motions and inertial sensors.

ACKNOWLEDGEMENTS

This work was supported in part by the Major Basic Research Project (5140503A0301), the National Natural Science Foundation of China (42174050), the Provincial and Municipal "Double First-Class" Construction Project (600460035), and the Hubei Luojia Laboratory Special Fund.

REFERENCES

Aggarwal, P., 2010. MEMS-based integrated navigation. Artech House

Dieter, W. R., Datta, S., & Kai, W. K. (2005, August). Power reduction by varying sampling rate. In Proceedings of the 2005 international symposium on Low power electronics and design (pp. 227-232).

Godha, S., 2006. Performance evaluation of low cost MEMS-based IMU integrated with GPS for land vehicle navigation application. UCGE report, (20239)

Lee, J. K., & Choi, M. J. (2018). Effect of strapdown integration order and sampling rate on IMU-based attitude estimation accuracy. Sensors, 18(9), 2775.

Li, Q., Ban, Y., Niu, X., Zhang, Q., Gong, L., & Liu, J. (2015).

Efficiency improvement of kalman filter for gnss/ins through one-step prediction of matrix. Mathematical Problems in Engineering, 2015.

Li, Y., Niu, X., Zhang, Q., Cheng, Y., & Shi, C. (2012, September). Observability analysis of non-holonomic constraints for land-vehicle navigation systems. In Proceedings of the 25th International Technical Meeting of the Satellite Division of The Institute of Navigation (ION GNSS 2012) (pp. 1521-1529)

Lo'ai, A. T., Basalamah, A., Mehmood, R., & Tawalbeh, H. (2016). Greener and smarter phones for future cities: Characterizing the impact of GPS signal strength on power consumption. IEEE Access, 4, 858-868.

Niu, X., Zhang, H., Shi, C., Chiang, K. W., & El-Sheimy, N. (2010, October). A proposed evaluation standard for the navigation results of MEMS INS/GPS integrated systems. In Proceedings of the International Symposium on GPS/GNSS (pp. 1-5).

Noureldin, A., Karamat, T. B., & Georgy, J. (2013). Fundamentals of inertial navigation, satellite-based positioning and their integration.

Shin, E. H., & El-Sheimy, N. (2002, January). Accuracy improvement of low cost INS/GPS for land applications. In Proceedings of the 2002 national technical meeting of the institute of navigation (pp. 146-157).

Yan, P., Jiang, J., Tang, Y., Zhang, F., Xie, D., Wu, J., ... & Liu, J. (2021). Dynamic Adaptive Low Power Adjustment Scheme for Single-Frequency GNSS/MEMS-IMU/Odometer Integrated Navigation in the Complex Urban Environment. Remote Sensing, 13(16), 3236.

Zhang, Q., Niu, X., & Shi, C. (2019). Assessment of the effect of GNSS sampling rate on GNSS/INS relative accuracy on different time scales for precision measurements. Measurement, 145, 583-593.

This contribution has been peer-reviewed.
https://doi.org/10.5194/isprs-archives-XLVI-3-W1-2022-205-2022